HHS Public Access

Author manuscript

*ACS Appl Mater Interfaces*. Author manuscript; available in PMC 2018 December 28.

Published in final edited form as:

*ACS Appl Mater Interfaces*. 2018 September 26; 10(38): 31988–31997. doi:10.1021/acsami.8b11811.

# Protein Nanofibril Assemblies Templated by Graphene Oxide Nanosheets Accelerate Early Cell Adhesion and Induce Osteogenic Differentiation of Human Mesenchymal Stem Cells

**Yajun Shuai**[†,‡,§], **Chuanbin Mao**[*,†,§], and **Mingying Yang**[*,†]

[†]College of Animal Science, Zhejiang University, Hangzhou, Zhejiang 310058, China

[‡]School of Materials Science and Engineering, Zhejiang University, Hangzhou, Zhejiang 310027, China

[§]Department of Chemistry & Biochemistry, Stephenson Life Sciences Research Center, Institute for Biomedical Engineering, Science and Technology, University of Oklahoma, 101 Stephenson Parkway, Room 3310, Norman, Oklahoma 73019-5300, United States

## Abstract

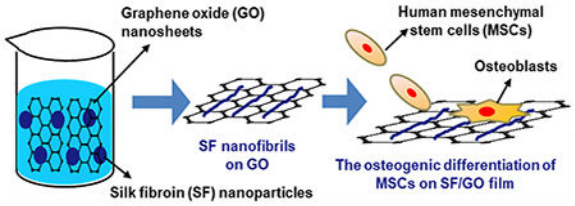


*Bombyx mori* silk fibroin (SF) is a promising natural biocompatible protein. However, its interaction with graphene oxide (GO) has never been studied and the resultant SF/GO matrix has not been used to direct stem cell fate. Herein, we found out that mixing SF molecules and GO nanosheets in an aqueous solution can trigger the assembly of SF nanoparticles into oriented nanofibrils due to the guidance of GO nanosheets, forming SF/GO films with unique nanotopographies and improved modulus upon the removal of the solvent. When GO mass percentage in the SF/GO films is 2 and 10%, the SF assemblies are necklace-like nanofibrils (assembled from loosely linked SF nanoparticles) and solid nanofibrils (assembled from densely linked SF nanoparticles) in the resultant films, termed SG2 and SG10, respectively. GO nanosheets guided the SF assembly into nanofibrils by triggering the structural change of SF molecules from random coils to $\beta$-sheets, as confirmed by Fourier transform infrared spectroscopy and circular dichroism measurements. Furthermore, oxidative groups in the GO nanosheets were reduced by the reducing groups in SF during the nanofibril formation according to X-ray photoelectron spectroscopy and Raman spectroscopy. The reduction of the oxidative groups in GO by SF was further verified by the good cell viability on the SF/GO films. The unique nanotopographies of the

[*]**Corresponding Authors**: cbmao@zju.edu.cn (C.M.). yangm@zju.edu.cn (M.Y.).

Supporting Information

The Supporting Information is available free of charge on the ACS Publications website at DOI: 10.1021/acsami.8b11811.

$R_a$ and $R_q$ of samples; Raman spectra of samples; and FTIR spectra of samples (PDF)

The authors declare no competing financial interest.

SF/GO films were found to accelerate the early cell adhesion and induce the osteogenic differentiation of human mesenchymal stem cells (MSCs) even in the absence of additional inducers in the medium. More importantly, SG10 presents a stronger capability in promoting early MSC adhesion by promoting F-actin assembly, increasing cell spreading area, and inducing the osteogenic differentiation of the MSCs by the unique SF/GO nanofibrous matrix. To the best of our knowledge, it is the first report that the SF/GO substrates can induce the osteogenic differentiation of MSCs in the absence of osteogenic differentiation medium. Therefore, SF/GO composite materials would have a potential application in the field of bone tissue engineering.

**Keywords**

silk fibroin; graphene oxide; mesenchymal stem cells; cell–substrate interactions; osteogenic differentiation; bone tissue engineering

## 1. INTRODUCTION

Designing artificial biomaterials is a promising approach to bone defect repair and regeneration. This strategy aims to design a scaffold mimicking the nanofibrous structure of extracellular matrix (ECM) to regulate cell adhesion, proliferation, signal transduction, and differentiation for repair or regeneration of bone tissue in vivo.[1] ECM mediates human mesenchymal stem cells (MSCs) differentiation by virtue of its reasonable distribution of nanofibers and the component proteins. Namely, ECM nanofibers and ECM compositions are described as biophysical factors such as nanotopographical structures and biochemical factors, respectively.[2–4] Therefore, a fine selection of material composition and subtle design of nanotopography have to be considered for the development of artificial ECM for bone tissue engineering.

Silk fibroin (SF) is a natural protein spun from *Bombyx mori* silkworm. It has favorable properties including biodegradability, mechanical superiority, processibility, and biocompatibility that can meet the requirements of scaffolds for regenerative medicine,[5–7] enabling its potential application in regenerative medicine.[8–10] The mechanical property and roughness characteristic of silk protein substrates can affect the adhesion of MSCs.[11,12] Further research has found out that the topographical surface of silk protein substrates can not only influence the adhesion and morphology of MSCs but also direct osteogenic differentiation of MSCs.[13] This implies that controlling the nanotopography of silk protein-based scaffolds as well as their mechanical properties might regulate the osteogenic differentiation of MSCs.

Interestingly, graphene oxide (GO), an atomically thin material, provides reactive sites for functionalization because of its abundant functional groups and high surface area.[14] Increasing evidence indicates peculiar functional groups from GO play an important function in regulating cell behaviors.[15–17] On the other hand, attempts have been made to forming GO and SF composites, but the resultant composites usually do not resemble nanofibrous ECM[18,19] and also are formed under harsh conditions such as alkaline pH, long incubation time, and high-temperature treatment.[19–22] Moreover, how to assemble SF into nanofibrils, which form an ECM-like matrix on the GO nanosheets, by using GO nanosheets

as templates at facile conditions, has not been studied. Additionally, our previous study shows that SF films surface having nanoridges can induce osteogenic differentiation of MSCs when osteogenic inducers are not added.[11] However, there is no report on answering whether the GO-templated SF nanofibrils would impact the adhesion or osteogenic differentiation of MSCs in the presence and absence of osteogenic factors.

Hence, we invented a facile one-step process by mixing GO nanosheets and SF with an appropriate ratio for inducing the self-assembly of SF nanofibrils at room temperature and in the neutral aqueous solution (Scheme 1A,B). The SF/GO films were obtained by casting the resultant SF/GO mixture on the polystyrene Petri dishes (Scheme 1C). After human MSCs were seeded sparsely (Scheme 1D) onto the SF/GO films, we hypothesized that the nanotopography of the SF/GO films could regulate the cell behavior together by altering the ECM clustering, focal adhesions (FAs), and cytoskeletal organization of MSCs (Scheme 1 E), further leading to changes in the cell phenotype and cell differentiation process (Scheme 1F).

## 2. MATERIALS AND METHODS

### 2.1. Preparation of SF Solution.

The fresh SF solution was prepared according to our previously reported protocol.[23] Briefly, tiny pieces of *B. mori* cocoon shells were boiled twice in 0.5% $Na_2CO_3$ aqueous solution for 0.5 h for removing sericin from cocoons. After drying, the SF fibers were gradually dissolved in 9.3 M LiBr aqueous solution and then dialyzed against distilled water for 72 h for obtaining aqueous SF solution. The SF solution concentration was calculated by the weighing method.

### 2.2. Self-Assembly of SF and GO.

**2.2.1. Morphology of SF/GO Composites in Aqueous Solution.—**For observation of assembled SF morphology induced by GO (Hengqiu Graphene Tech Co. Ltd, China), the SF/GO solution was diluted in deionized water to reach the desired concentration (0.01 mg/L), and 5 μL of the solution was dropwise added on the freshly peeled mica disc and air-dried. The self-assembly morphology of SF/GO was observed using an atomic force microscopy (AFM) system (VEECO MultiMode, USA).

**2.2.2. Structure Characterization of SF/GO Composites.—**The circular dichroism (CD) spectra of the SF/GO composites were measured from 190 to 250 nm at the rate of 0.5 nm/s using a MOS-450 Spectrometer (Biologic, France). X-ray photoelectron spectroscopy (XPS) was observed by using an X-ray photoelectron spectrometer (ESCALAB 250Xi, Thermo Fisher Scientific). Raman spectra and Raman scanning images were obtained by Raman microscopy (DXR2, Thermo Fisher Scientific) using a 532 nm laser.

### 2.3. Fabrication of SF/GO Films.

The GO solution with a concentration of 2 mg/mL was dispersed by ultrasonication for 20 min to form a homogeneous GO dispersion. The concentration of SF solution was adjusted to be 100 mg/mL. After the GO solution was added into SF solution, a homogeneous

suspension was finally obtained after continuously stirring the mixture for 30 min. Here, the mass percentage of GO with respect to SF in the suspension was adjusted to be 2 or 10% (when the total mass percentage of GO and SF is considered 100%). To prepare the SF/GO films, 5 mL of SF/GO composite solutions was poured into polystyrene Petri dishes and subsequently air-dried for 48 h to form SF/GO films. The SF/GO films containing 2% GO and 10% GO were denoted as SG2 and SG10, respectively.

## 2.4. Characterization of SG2 and SG10 Films.

### 2.4.1. Mechanical Property of SG2 and SG10.—

The mechanical properties of the films were determined using a universal testing machine (AGS-J, Shimadzu, Japan) at a temperature of 25 °C and humidity of 80% with a 10 N capacity load cell. The films were cut into a dumbbell shape of 0.4 cm × 2 cm for the tensile tests. The specimens were stretched at a speed of 0.1 mm/s.

### 2.4.2. Fourier-Transform Infrared Spectroscopy (FTIR) of SG2 and SG10.—

The films were pressed into discs mixed with KBr powder and evaluated using a FTIR (FTIR-8400S, Shimadzu, Japan) according to our previous methods.[24] A curve fitting and Fourier self-deconvolution treatment of the amide I region (1600–1710 $cm^{-1}$) was carried out to quantitatively estimate the relative proportion of silk secondary structures. The amount of individual secondary structure element was calculated, through dividing the relative peak areas of one amide I band by the total peak areas of all amide I bands using the Origin software peak-fitting module (Origin 8).[25]

### 2.4.3. Contact Angle Measurements of SG2 and SG10.—

The surface wettability of SG2 and SG10 films was evaluated at room temperature through a drop shape analysis system coupled with a computer-assisted contour analysis program (OCA20, DataPhysics Corp, Germany).

## 2.5. Cell Viability Assay and Cell Morphology.

Human MSCs (Cyagen Biosciences, China) were cultured in serum-containing medium (HUXMA-90011, Cyagen Biosciences). The SG2 and SG10 film were fixed on the bottom of 24-wells plates. SF film, tissue culture plate (TCP), and GO coating on the TCP were set as the control group. Adding 75% (V/V) ethanol into each well sterilized the films, which were further washed three times using a phosphate buffer solution (PBS). The cell numbers were counted using a handheld automated cell counter (Millipore, USA). Cells at a density of $2.0 \times 10^4$ cells/$cm^2$ were immediately seeded in 24-well plates which were coated with different films.

### 2.5.1. AlamarBlue Assays.—

The cell viability on the SF/GO films was determined by using alamarBlue cell viability reagent kit (Life Technologies). After MSCs were cultured for 1 and 5 d, 10 μL of alamarBlue solution was added and incubated for another 3 h at 37 °C. A microplate reader was used to quantify the cell viability as relative fluorescence units (RFU) by monitoring fluorescence with an excitation and emission wavelength of 530 and 600 nm, respectively.

**2.5.2. Cell Morphology.—**Cells were fixed in fixative (Beyotime Institute of Biotechnology, China) for 1 h and washed three times by PBS. After fixation, the cytoskeletons were stained with Alexa Fluor 488 phalloidin (Invitrogen), and cell nuclei were visualized by DAPI (Beyotime Institute of Biotechnology, China) at room temperature. Cell morphology was acquired using a confocal microscope system (Zeiss LSM780, Germany).

**2.5.3. Cell Adhesion.—**Cells ($1.0 \times 10^5$) were seeded in 24-wells. After they were cultured for different times (0.5 and 3 h), PBS solution was used to wash them three times in order to get rid of the non-adherent cells. After that, each well was fixed with fixative solution for 20 min and soaked in 1% Triton X-100 for 10 min, followed by incubation with Fluor 480 phalloidin dye for 30 min and DAPI for 10 min in the dark, and finally placed under an optical microscope to observe the cell adhesion. Statistical analysis was used to calculate the number of cells and the cell spread area based on the images by Image-Pro Plus software. For immunofluorescence staining of cell adhesion proteins (vinculin and paxillin), MSCs were cultured for 2 d and fixed in 4% paraformaldehyde at room temperature, then permeabilized by 0.2% Triton X-100. They were subsequently incubated first with 4% bovine serum albumin/PBS for 30 min and then with specific primary antibodies (Anti-Vinculin [VLN01, Invitrogen] and Anti-Paxillin [Y113, Abcam]) overnight at 4 °C. They were then incubated with the secondary antibodies conjugated with Alexa Fluor 488 (Abcam, ab150117) and Alexa Fluor 594 (Abcam, ab150080), respectively, and stained by DAPI for probing the cell nuclei.

## 2.6. Osteogenic Differentiation of MSCs on SG2 and SG10.

MSCs in a low density ($2.0 \times 10^4$ cells/well) were implanted on these SF/GO matrixes and then cultured in the osteogenic induction medium (containing: primary media, 50 $\mu$M ascorbic acid, 10 mM beta-glycerol phosphate, and 100 nM dexamethasone) or in the normal medium (serum-containing medium supplemented with 50 mM of $CaCl_2$) for 14 d. For real-time polymerase chain reaction (PCR), the mRNA levels of integrin $\alpha 2$ (Itg$\alpha 2$) and collagen type I (COLI) of MSCs cultured on the composite films in the osteogenic medium were assessed. All primers (Sangon Biotech) were designed and are listed in Table 1 for the PCR quantification with GAPDA as a reference gene. For immunofluorescence staining of osteogenic differentiation-related proteins, including COLI, osteocalcin (OCN), and osteopontin (OPN), MSCs on the SF/GO films were fixed in a fixative solution for 30 min at room temperature. Then, the MSCs were probed with the primary antibodies of anti-collagen type I (ab34710, Abcam), anti-OCN (ab13418, Abcam), and anti-OPN (ab8448, Abcam) overnight at 4 °C, followed by staining with secondary antibody conjugated with Alexa Fluor 488 (ab150117, Abcam) or Alexa Fluor 594 (ab150080, Abcam). After incubation with the secondary antibody, the MSCs were stained by DAPI for probing the cell nuclei. In addition, alkaline phosphatase (ALP) staining (BCIP/NBT staining kit, Beyotime) and alizarin red staining (Alizarin Red S, Sigma) were also carried out according to the previous procedure[26] to investigate the osteogenic differentiation of MSCs.

### 2.7. Statistical Analysis.

One-way analysis of variance was used to statistically analyze the data, which were represented in the form of mean ± standard deviation (SD). When the *P*-value was less than 0.05 and 0.01, the difference between different groups was thought statistically and extremely significant, respectively.

## 3. RESULTS

### 3.1. Assembly of SF into Nanofibrils Induced by the GO Template.

The representative AFM height images (Figure 1A–H) showed the nanotopography of SF, GO nanosheets, and SF/GO composites. Figures 1A,B shows that freshly prepared SF formed nanoparticles with an uneven size. Figure 1C,D shows that the GO nanosheets had a planar surface and polygonal morphology. Interestingly, adding GO into SF solution drove SF to be self-assembled into different nanotopographies, depending on the GO mass percentage in the GO/SF composites (Figure 1E–H). At a GO percentage of 2%, SF nanoparticles were loosely linked and assembled into necklace-like nanofibrils (Figure 1F). The necklace-like nanofibrils formed an oriented head-to-tail structure, proving the oriented assembly of SF nanoparticles with the guidance of the GO templates. Increasing the GO percentage to 10% resulted in the formation of densely packed solid SF nanofibrils (assembled from densely linked SF nanoparticles) on the GO nanosheets (Figure 1G). The high magnification view of the nanofibrils on the GO nanosheets (Figure 1H) confirmed that the nanofibrils were indeed assembled from SF nanoparticles. Therefore, AFM images clearly demonstrated that SF was assembled into nanofibrils and the nanotopography of the resultant nanofibrous substrate, either loosely linked necklacelike or densely linked solid nanofibrils, could be regulated by varying the proportion of SF/GO. The detailed results of section analysis collected along with the AFM traces (Figure 1I–L) and surface roughness analysis (Figure S1A,B) showed that the ordered assembly of SF on GO nanosheets was due to the binding of SF by the GO at the specific sites. These findings proved that a suitable percentage of GO in the SF/GO films played an important role in directing the assembly of SF into the varying nanotopography.

To further prove that the assembly of the SF was triggered by GO, CD spectra, Raman spectra, and XPS spectra were measured. Figure 2A,B shows the CD spectra of SF and SF/GO solutions. Fresh SF had a random coil conformation according to a negative ellipticity at about 200 nm (Figure 2A). After the GO was mixed with SF by increasing its proportion from 2 to 10%, the decrease of the peak at 200 nm and the increase of peak at 218 nm proved that the percentage of $\beta$-sheet structure was increased with the increase in the GO content (Figure 2A,B), indicating that the GO could dramatically affect the secondary structure of SF. It should be noted that the $\beta$-sheet structure of SF favors the assembly of SF nanofibrils.[27] Therefore, CD spectra proved that the secondary structure of SF could be mediated by changing the GO content in the neutral aqueous solution. In addition, Raman spectroscopy (Figure S2) showed that the intensity ratio ($I_D$ band/$I_G$ band) of SG10 was higher than that of GO, indicating that the GO in SG10 solution was chemically reduced. In order to analyze these changes in the GO/SF composites more carefully, we used the XPS technique to detect the C 1s spectra of GO/SF composites

(Figure 2C–F). Figure 2D–F shows that the oxygen species (C–O and O–C═O) from GO nanosheets were reduced by SF after the GO was added to the SF solution, indicating that the SF could be used as a reducing agent to reduce GO. Hence, our findings prove that the interaction between SF and GO drives the self-assembly of SF nanofibrils on the GO nanosheets and promotes the reduction process of GO in neutral pH conditions.

### 3.2. Characterization of SF/GO Films.

Figure 3A shows the photographs of the obtained SF, SG2, and SG10 films. Figure 3B shows that the Young's moduli of SG2 and SG10 films were 240 and 270 MPa, respectively, higher than that of the SF film (210 MPa). Increasing the concentration of GO resulted in an increase in the Young's modulus of SF/GO films. Therefore, the mechanical properties of SF/GO can be slightly changed by controlling the ratio of GO and SF.

As the secondary structure is one of the important factors determining the mechanical properties, we characterized the secondary structure with FT-IR for clarifying mechanical properties of SF, SG2, and SG10 films. Figure S3 shows that the SF film adopted a predominantly random coil conformation. With more GO added into SF, the absorption peaks of amide I and amide II were all right-shifted, indicating the structural transformation of SF from random coils to $\beta$-sheets. In addition, deconvolution of the overlapped peaks to resolve amide I in the region of 1600–1700 $cm^{-1}$ was performed based on peak assignment that 1623–1641 and 1675–1700 $cm^{-1}$ were assigned to $\beta$-sheets, 1656–1662 $cm^{-1}$ to $\alpha$-helices, 1642–1655 $cm^{-1}$ to random coils, and 1663–1674 $cm^{-1}$ to turns.[28,29] Figure 4A–C shows the detailed secondary structures of SF/GO films. The curve fitting result in percentage terms (Figure 4D) indicated that SF had the lowest $\beta$-sheets content at around 25.13%. After the GO was added, the $\beta$-sheet content was increased to 60.04 and 74.39% for SG2 and SG10, respectively. FTIR results confirmed that the GO template could trigger the $\beta$-sheets assembly of SF. In addition, the wettability of SF/GO films was measured because material compositions and geometric structure strongly influenced the wettability of a biomaterial surface. The contact angles of SF, SG2, and SG10 films were 71.4°, 76.7°, and 80.0° (Figure 4E), respectively. The SG10 films had a contact angle higher than the SF films, indicating that the SG10 films were less hydrophilic probably because of the decrease of oxy-compound groups from GO and the increase of $\beta$-sheets of SF as a result of the interaction between SF and GO.

### 3.3. Cell Viability and Adhesion of MSCs.

To study how SF/GO films would play a role in the cell viability and adhesion, we seeded MSCs on the SF/GO films and then measured cell proliferation ability by alamarBlue assay (Figure 5A). Figure 5A shows that the values of the RFU increased over time for each group, indicating an increase in the cell number cultured on the substrate throughout the cell culture period. Cells cultured for 5 d showed a higher cell number on the SF/GO films than the GO films without a statistical difference. Therefore, cell proliferation analysis suggested that SF/GO and GO films could serve as a biomaterial to maintain cell growth. In addition, cellular morphology was observed by staining the F-actin cytoskeleton in Figure 5B. The confocal micrographs indicated that MSCs exhibited a more elliptical-patterned phenotype on the TCP, SF films, and GO films on day 1. Interestingly, more spindle-shaped

morphology and obvious filopodia extensions of MSCs could be observed on the SG2 and SG10 films. After 5 d of culturing, the morphology of MSCs on the TCP and SF films still exhibited an elliptical-patterned or irregular phenotype, suggesting that the SF/GO matrix exerted a significant influence on the assembly of the F-actin cytoskeleton.

To further understand the early adhesion behavior of MSCs on the SF/GO matrix, we observed the adhesion morphology of MSCs and tracked the adhesion-associated proteins. Figure 6A shows that the MSCs were spheroidal on all groups after adhesion for 0.5 h. However, the SG10 group had more cells than the SF group and SG2 group (Figure 6A,D), indicating that the SG10 film had the ability in promoting early cell adhesion. After 3 h of adhesion, the number of cells on the SF and SG2 films remained low (Figure 6B,E). Interestingly, after 3 h of attachment, the average cell spreading area of MSCs on the SG10 film was larger than that on the TCP, indicating that the SG10 films could promote cell adhesion in the early stage (Figure 6G). Next, FA formation of MSCs, which served as the mechanical links to the SF/GO matrix, was further examined by labeling two adhesion-associated proteins: vinculin and paxillin. As shown in Figure 6C, vinculin and paxillin were localized predominantly at the cell periphery on the SG10 films. However, they were localized at the nucleus periphery on the SF films, indicating that MSCs on the SF films lacked filopodia extensions. These results showed that SG10 substrates played a role in facilitating cell adhesion and signal transduction of FAs.

### 3.4. Osteogenic Differentiation and Cellular Matrix Expression of MSCs.

To examine the effect of SF/GO films on the differentiation of MSCs, we seeded MSCs on the SF/GO films in the presence and absence of osteogenic inducers. Integrin $\alpha 2$ belongs to the integrin alpha subunit family that is responsible for cell adhesion, stress-fiber formation, and organization of ECM and also participates in the early osteogenic differentiation.[30,31] When incubated in the medium having osteogenic inducers, the RT-PCR showed that the SG2 and SG10 films had a higher level of Itg$\alpha 2$ than the control groups (Figure 7A), and the SG10 film had the highest level of COLI expression (Figure 7B) after culturing 14 d, suggesting that SF/GO films could promote the expression of ECM proteins. In addition, we seeded MSCs in the medium in the absence of osteogenic inducers to evaluate the induction efficiency of osteogenic differentiation by the SF/GO films. Higher levels of ALP staining (Figure 7D) and alizarin red staining (Figure 7C,E) were observed on the SG10 films. Quantitative alizarin red staining (Figure 7C) results showed that the staining area on the SG10 films was higher than that on the TCP. Moreover, immunofluorescence staining of COLI, OPN, and OCN confirmed the matrix staining results (Figure 7F). MSCs cultured on all of the groups had recognizable COLI-positive and OPN-positive staining. Furthermore, MSCs cultured on the SG10 films expressed significantly more OCN proteins that those on other groups on day 14, suggesting that the SG10 film could induce the osteogenic differentiation of MSCs. Taken together, these results consistently verified that the SG10 substrate provides more suitable microenvironment than the SG2 films in accelerating the early adhesion and inducing the osteogenic differentiation of MSCs when osteogenic inducers were absent in the medium.

## 4. DISCUSSION

So far, the interaction between SF and GO that drives the assembly of SF as well as the application of the resultant SF/GO composites has not been studied. In addition, to date whether such SF/GO composites could regulate the fates of stem cells is poorly understood. For this purpose, we designed a novel approach to the preparation of SF/GO matrix and characterized the structural properties of the resultant SF/GO matrix by CD, FTIR, and XPS measurements. We also seeded human MSCs on the resultant SF/GO matrix and investigated the in vitro performance of the cell adhesion, proliferation, and differentiation of MSCs.

When a SF molecule forms a steric structure, its polypeptide chain mainly forms random coils and $\alpha$-helix structures and thereby is further folded into a spherical nanoparticle.[23] In the present study, AFM data (Figure 1) directly showed that SF nanoparticles were assembled into nanofibrils nearly aligned on the GO nanosheets when the GO proportion was increased from 2 to 10% (Figures 1 and S1). Ling et al. considered that amphiphilic SF molecules could interact with the C–C $sp^2$-hybridized carbon surfaces on the GO.[21] Some amino acids such as valine, isoleucine, and threonine from proteins can destabilize $\alpha$-helix to form $\beta$-sheets by changing solution conditions,[32] indicating that GO substrates might interact with such amino acids in SF to promote the $\beta$-sheets formation and the subsequent SF assembly. Indeed, the CD, XPS, and FTIR analysis (Figures 2 and 4) proved that more $\beta$-sheet structures in the SF molecules were formed with the addition of GO while the oxidative groups of GO were also reduced by the SF. These results suggest that the higher specific surface area of GO with lots of oxidative groups can promote the interaction with the amino acids inside the SF, favoring the change of the secondary structures of SF from $\alpha$-helix to $\beta$-sheets. Driven by the intermolecular hydrogen bonding, the SF with $\beta$-sheet structures could undergo self-assembly on the GO nanosheets to form an ordered fibril structure.[33]

Many studies have shown that the compositions of secondary structure, surface functional groups, and roughness characteristics can affect the surface hydrophilicity of polymer substrates.[11,34,35] The contact angle measurements showed that the increasing of $\beta$-sheet structures of SF and the reduction of oxidative groups made the SG10 films more hydrophobic (Figure 4E). The formation of SF/GO complex also slightly improved the modulus of the biomaterials, consistent with the earlier findings that more $\beta$-sheet structures in the SF would lead to improved mechanical properties of the SF-derived materials.[36,37] The primary sequence of the SF protein consists of alternating hydrophobic and hydrophilic fragments. The spatial arrangement of these fragments can affect the hydrophilic properties and mechanical strength of the SF molecules.[38] In addition, a large body of literature studies show that the oxy-compound groups of GO can promote cellular behaviors.[39–42] In our study, GO coating indeed showed the excellent biocompatibility in the SF/GO films (Figure 5). Therefore, the SF/GO matrix we designed in this study can improve the overall performance needed in biomedical applications of the SF/GO composite materials.

It was previously reported that morphology can induce an guide the differentiation of stem cells.[11,13,43] In this study, SF/GO films with different GO content presented two different nanotopographies. Namely, the SG2 and SG10 presented necklace-like and solid nanofibrils

on the GO nanosheets, respectively. Because nanotopographical properties of the substrate surface can directly affect the cell behaviors, we first investigated the role of the nanotopographical cues created by the SF/GO films in regulating the adhesion of MSCs. We found that many cells started to adhere on the SF/GO films 0.5 h after cell seeding (Figure 6A) and presented an elongated cytoskeleton feature after 1 d of culturing (Figure 5B). More importantly, the SG10 films more favored the early cell adhesion than the SG2 films because the former had a unique more nanofibrous structure than the latter. This interesting result prompted us to know how the MSCs adhered to the SF/GO matrixes. Vinculin and paxillin are expressed for the aggregation assembly of membrane cytoskeletons, which is often related to the formation of FAs and increasing of cytoskeletal contractility.[44] We found that MSCs assembled FAs along the cell margins rather than around the nuclei for the cells on the SF/GO films and more FAs were formed on the SG10 than SG2 films (Figure 6C). Therefore, these findings indicated that ECM-like nanofibrous structures of the SF/GO films (SG10 in particular) facilitated the early cell adhesion and stimulated the organization of the cytoskeleton that resulted in the changes of cellular morphology.

Because of the morphological changes of the MSCs on the SF/GO films, the subsequent cell fate such as differentiation will also be affected. Figure 7 shows that the osteogenesis-related markers of MSCs, such as integrin $\alpha 2$ and OCN, on the SF/GO films were significantly upregulated (with the MSCs on the SG10 films being more upregulated than those on the SG2 films) compared with the control group. Studies have shown that the enhanced formation of FAs contributed to the osteoblastic differentiation of MSCs.[45] The theory of anchoring cell-fate cues is critical to understand the general effects of the SF/GO films on the MSCs adhesion and differentiation.[46] SF nanofibrils aligned on the GO nanosheets in the SG10 group provided more abundant anchoring points for the MSCs adhesion and the FA formation than the necklace-like nanofibrils in the SG2 group. When the anchoring points were more tightly bound, they provided enough mechanical feedback to MSCs and resulted in improved cytoskeletal rearrangement in MSCs (Scheme 1E). It was proposed that the substrate morphologies directed differentiation by affecting the cellular mechanotransductions and related signaling pathways of stem cells and cancer cells.[46–48] As a result, the rearrangement of cytoskeletons and activation of the signaling pathway of the extracellular-signal-related kinase/mitogen-activated protein kinase of MSCs on the ECM-like substrate could further stimulate the down-stream signaling to promote stem cell differentiation.[46] This nanotopography-related mechanism is the possible reason why the SG10 films with aligned solid nanofibrils showed a higher capability in inducing the osteogenic differentiation than the SG2 films with necklace-like nanofibrils. Namely, our results indicate that the nanotopography of the SG10 films contributed significantly to the induced osteogenic differentiation. Overall, our results about cell adhesion and differentiation confirmed the underlying mechanisms by which the unique nanofibrous SG10 films favored the cell adhesion and differentiation.

## 5. CONCLUSIONS

In summary, we discovered that the GO could effectively serve as a platform for the site-specific assembly and growth of SF nanofibrils in aqueous solution by a facile one-step process. This finding proves that the hydrophilic GO can interact with SF molecules and

assemble them into aligned nanofibrils. More GO addition to the SF solutions promoted the assembly and β-sheet transition of SF nanofibrils as well as the reduction of the oxidative groups in GO by SF. The resultant SF/GO films were biocompatible, exhibited a good mechanical property, and accelerated MSCs growth. Most importantly, for the first time, we found that the SF/GO films provided a unique nanofibrous matrix favoring the early adhesion and inducing the osteogenic differentiation of MSCs. These results suggest that the nanotopographical properties of SF/GO substrate could be dominant in determining the organization of the cell adhesion, followed by promoting the osteogenic differentiation of MSCs. Therefore, our study has a major impact on the design of biomaterials and convincingly proves that SF/GO scaffolds could be potentially employed in inducing bone tissue formation for bone repair.

## Supplementary Material

Refer to Web version on PubMed Central for supplementary material.

## ACKNOWLEDGMENTS

The authors acknowledge the support of Zhejiang Provincial Natural Science Foundation of China (LZ17C170002 and LZ16E030001), National Natural Science Foundation of China (51673168, 81871499, and 31800807), State of Sericulture Industry Technology System (CARS-18-ZJ0501), Zhejiang Provincial Science and Technology Plans (2016C02054-19), the National Key Research and Development Program of China (2016YFA0100900), and China Postdoctoral Science Foundation (2018M630678). Y.J.S. and C.B.M. would also like to thank the financial support from National Institutes of Health (CA200504, CA195607, and EB021339).

## REFERENCES

(1). Tang D; Tare RS; Yang L-Y; Williams DF; Ou K-L; Oreffo ROC Biofabrication of Bone Tissue: Approaches, Challenges and Translation for Bone Regeneration. Biomaterials 2016, 83, 363–382. [PubMed: 26803405]

(2). Guilak F; Cohen DM; Estes BT; Gimble JM; Liedtke W; Chen CS Control of Stem Cell Fate by Physical Interactions with the Extracellular Matrix. Cell Stem Cell 2009, 5, 17–26. [PubMed: 19570510]

(3). Derby B Printing and Prototyping of Tissues and Scaffolds. Science 2012, 338, 921–926. [PubMed: 23161993]

(4). Pati F; Song T-H; Rijal G; Jang J; Kim SW; Cho D-W Ornamenting 3D Printed Scaffolds with Cell-Laid Extracellular Matrix for Bone Tissue Regeneration. Biomaterials 2015, 37, 230–241. [PubMed: 25453953]

(5). Wang Y; Kim H-J; Vunjak-Novakovic G; Kaplan DL Stem Cell-Based Tissue Engineering with Silk Biomaterials. Biomaterials 2006, 27, 6064–6082. [PubMed: 16890988]

(6). Farokhi M; Mottaghitalab F; Shokrgozar MA; Kaplan DL; Kim H-W; Kundu SC Prospects of Peripheral Nerve Tissue Engineering Using Nerve Guide Conduits Based on Silk Fibroin Protein and Other Biopolymers. Int. Mater. Rev 2017, 62, 367–391.

(7). Farokhi M; Mottaghitalab F; Samani S; Shokrgozar MA; Kundu SC; Reis RL; Fatahi Y; Kaplan DL Silk Fibroin/Hydroxyapatite Composites for Bone Tissue Engineering. Biotechnol. Adv 2017, 36, 68–91. [PubMed: 28993220]

(8). Yang M; Zhou G; Shuai Y; Wang J; Zhu L; Mao C Ca2+-induced self-assembly of Bombyx mori silk sericin into a nanofibrous network-like protein matrix for directing controlled nucleation of hydroxylapatite nano-needles. J. Mater. Chem. B 2015, 3, 2455–2462. [PubMed: 26029374]

(9). Correia C; Bhumiratana S; Yan L-P; Oliveira AL; Gimble JM; Rockwood D; Kaplan DL; Sousa RA; Reis RL; Vunjak-Novakovic G Development of Silk-Based Scaffolds for Tissue Engineering

of Bone from Human Adipose-Derived Stem Cells. Acta Biomater. 2012, 8, 2483–2492. [PubMed: 22421311]

(10). Chouhan D; Thatikonda N; Nilebäck L; Widhe M; Hedhammar M; Mandal BB Recombinant Spider Silk Functionalized Silkworm Silk Matrices as Potential Bioactive Wound Dressings and Skin Grafts. ACS Appl. Mater. Interfaces 2018, 10, 23560. [PubMed: 29940099]

(11). Yang M; Shuai Y; Sunderland KS; Mao C Ice-Templated Protein Nanoridges Induce Bone Tissue Formation. Adv. Funct. Mater 2017, 27, 1703726. [PubMed: 29657571]

(12). Bai L; Zhu L; Min S; Liu L; Cai Y; Yao J Surface Modification and Properties of Bombyx Mori Silk Fibroin Films by Antimicrobial Peptide. Appl. Surf. Sci 2008, 254, 2988–2995.

(13). Yang M; Shuai Y; Zhou G; Mandal N; Zhu L; Mao C Tuning Molecular Weights of *Bombyx Mori* (*B. Mori*) Silk Sericin to Modify Its Assembly Structures and Materials Formation. ACS Appl. Mater. Interfaces 2014, 6, 13782–13789. [PubMed: 25050697]

(14). Sanchez VC; Jachak A; Hurt RH; Kane AB Biological Interactions of Graphene-Family Nanomaterials: An Interdisciplinary Review. Chem. Res. Toxicol 2011, 25, 15–34. [PubMed: 21954945]

(15). Nayak TR; Andersen H; Makam VS; Khaw C; Bae S; Xu X; Ee P-LR; Ahn J-H; Hong BH; Pastorin G; Özyilmaz B Graphene for Controlled and Accelerated Osteogenic Differentiation of Human Mesenchymal Stem Cells. ACS Nano 2011, 5, 4670–4678. [PubMed: 21528849]

(16). Kostarelos K; Novoselov KS Exploring the Interface of Graphene and Biology. Science 2014, 344, 261–263. [PubMed: 24744363]

(17). Akhavan O; Ghaderi E; Shahsavar M Graphene Nanogrids for Selective and Fast Osteogenic Differentiation of Human Mesenchymal Stem Cells. Carbon 2013, 59, 200–211.

(18). Hu K; Gupta MK; Kulkarni DD; Tsukruk VV Ultra-Robust Graphene Oxide-Silk Fibroin Nanocomposite Membranes. Adv. Mater 2013, 25, 2301–2307. [PubMed: 23450461]

(19). Hu K; Tolentino LS; Kulkarni DD; Ye C; Kumar S; Tsukruk VV Written-in Conductive Patterns on Robust Graphene Oxide Biopaper by Electrochemical Microstamping. Angew. Chem., Int. Ed 2013, 52, 13784–13788.

(20). Huang L; Li C; Yuan W; Shi G Strong composite films with layered structures prepared by casting silk fibroin-graphene oxide hydrogels. Nanoscale 2013, 5, 3780–3786. [PubMed: 23538717]

(21). Ling S; Li C; Adamcik J; Wang S; Shao Z; Chen X; Mezzenga R Directed Growth of Silk Nanofibrils on Graphene and Their Hybrid Nanocomposites. ACS Macro Lett 2014, 3, 146–152.

(22). Wang L; Lu C; Zhang B; Zhao B; Wu F; Guan S Fabrication and Characterization of Flexible Silk Fibroin Films Reinforced with Graphene Oxide for Biomedical Applications. RSC Adv 2014, 4, 40312–40320.

(23). Yang M; He W; Shuai Y; Min S; Zhu L Nucleation of hydroxyapatite crystals by self-assembled Bombyx mori silk fibroin. J. Polym. Sci., Part B: Polym. Phys 2013, 51, 742–748.

(24). Shuai Y; Yang S; Li C; Zhu L; Mao C; Yang M In situ protein-templated porous protein-hydroxylapatite nanocomposite microspheres for pH-dependent sustained anticancer drug release. J. Mater. Chem. B 2017, 5, 3945–3954. [PubMed: 29152304]

(25). Chadefaux C; Le Hô A-S; Bellot-Gurlet L; Reiche I Curve-Fitting Micro-ATR-FTIR Studies of the Amide I and II Bands of Type I Collagen in Archaeological Bone Materials. e-Preserv. Sci 2009, 6, 129–137.

(26). Yang M; Shuai Y; Zhang C; Chen Y; Zhu L; Mao C; OuYang H Biomimetic Nucleation of Hydroxyapatite Crystals Mediated by Antheraea Pernyi Silk Sericin Promotes Osteogenic Differentiation of Human Bone Marrow Derived Mesenchymal Stem Cells. Biomacromolecules 2014, 15, 1185–1193. [PubMed: 24666022]

(27). Su D; Yao M; Liu J; Zhong Y; Chen X; Shao Z Enhancing Mechanical Properties of Silk Fibroin Hydrogel through Restricting the Growth of $\beta$-Sheet Domains. ACS Appl. Mater. Interfaces 2017, 9, 17489–17498. [PubMed: 28470062]

(28). Lammel AS; Hu X; Park S-H; Kaplan DL; Scheibel TR Controlling Silk Fibroin Particle Features for Drug Delivery. Biomaterials 2010, 31, 4583–4591. [PubMed: 20219241]

(29). Lu Q; Hu X; Wang X; Kluge JA; Lu S; Cebe P; Kaplan DL Water-Insoluble Silk Films with Silk I Structure. Acta Biomater. 2010, 6, 1380–1387. [PubMed: 19874919]

(30). Hood JD; Cheresh DA Role of Integrins in Cell Invasion and Migration. Nat. Rev. Cancer 2002, 2, 91–100. [PubMed: 12635172]

(31). Glossop JR; Cartmell SH Differential Gene Expression of Integrins Alpha 2 and Beta 8 in Human Mesenchymal Stem Cells Exposed to Fluid Flow. Cell. Mol. Bioeng 2009, 2, 544–553.

(32). Ambroggio XI; Kuhlman B Design of Protein Conformational Switches. Curr. Opin. Struct. Biol 2006, 16, 525–530. [PubMed: 16765587]

(33). Xu S; Yong L; Wu P One-Pot, Green, Rapid Synthesis of Flowerlike Gold Nanoparticles/Reduced Graphene Oxide Composite with Regenerated Silk Fibroin as Efficient Oxygen Reduction Electrocatalysts. ACS Appl. Mater. Interfaces 2013, 5, 654–662. [PubMed: 23323590]

(34). Lai J; Sunderland B; Xue J; Yan S; Zhao W; Folkard M; Michael BD; Wang Y Study on Hydrophilicity of Polymer Surfaces Improved by Plasma Treatment. Appl. Surf. Sci 2006, 252, 3375–3379.

(35). Jiang J; Zhu L; Zhu L; Zhu B; Xu Y Surface Characteristics of a Self-Polymerized Dopamine Coating Deposited on Hydrophobic Polymer Films. Langmuir 2011, 27, 14180–14187. [PubMed: 22011109]

(36). Keten S; Xu Z; Ihle B; Buehler MJ Nanoconfinement controls stiffness, strength and mechanical toughness of $\beta$-sheet crystals in silk. Nat. Mater 2010, 9, 359–367. [PubMed: 20228820]

(37). Cho SY; Yun YS; Lee S; Jang D; Park K-Y; Kim JK; Kim BH; Kang K; Kaplan DL; Jin H-J Carbonization of a Stable $\beta$-Sheet-Rich Silk Protein into a Pseudographitic Pyroprotein. Nat. Commun 2015, 6, 7145. [PubMed: 25990218]

(38). Vepari C; Kaplan DL Silk as a Biomaterial. Prog. Polym. Sci 2007, 32, 991–1007. [PubMed: 19543442]

(39). Lee WC; Lim CHYX; Shi H; Tang LAL; Wang Y; Lim CT; Loh KP Origin of Enhanced Stem Cell Growth and Differentiation on Graphene and Graphene Oxide. ACS Nano 2011, 5, 7334–7341. [PubMed: 21793541]

(40). Ku SH; Park CB Myoblast Differentiation on Graphene Oxide. Biomaterials 2013, 34, 2017–2023. [PubMed: 23261212]

(41). Ruiz ON; Fernando KAS; Wang B; Brown NA; Luo PG; McNamara ND; Vangsness M; Sun Y-P; Bunker CE Graphene Oxide: A Nonspecific Enhancer of Cellular Growth. ACS Nano 2011, 5, 8100–8107. [PubMed: 21932790]

(42). Shin YC; Lee JH; Kim MJ; Hong SW; Kim B; Hyun JK; Choi YS; Park J-C; Han D-W Stimulating Effect of Graphene Oxide on Myogenesis of C2C12 Myoblasts on RGD Peptide-Decorated PLGA Nanofiber Matrices. J. Biol. Eng 2015, 9, 22. [PubMed: 26609319]

(43). Akhavan O Graphene Scaffolds in Progressive Nanotechnology/Stem Cell-Based Tissue Engineering of the Nervous System. J. Mater. Chem. B 2016, 4, 3169–3190.

(44). Wang J; Yang M; Zhu Y; Wang L; Tomsia AP; Mao C Phage Nanofibers Induce Vascularized Osteogenesis in 3D Printed Bone Scaffolds. Adv. Mater 2014, 26, 4961–4966. [PubMed: 24711251]

(45). Yang K; Jung H; Lee H-R; Lee JS; Kim SR; Song KY; Cheong E; Bang J; Im SG; Cho S-W Multiscale, Hierarchically Patterned Topography for Directing Human Neural Stem Cells into Functional Neurons. ACS Nano 2014, 8, 7809–7822. [PubMed: 25050736]

(46). Trappmann B; Gautrot JE; Connelly JT; Strange DGT; Li Y; Oyen ML; Stuart MAC; Boehm H; Li B; Vogel V; Spatz JP; Watt FM; Huck WTS Extracellular-Matrix Tethering Regulates Stem-Cell Fate. Nat. Mater 2012, 11, 642–649. [PubMed: 22635042]

(47). Shi X; Li L; Ostrovidov S; Shu Y; Khademhosseini A; Wu H Stretchable and Micropatterned Membrane for Osteogenic Differentation of Stem Cells. ACS Appl. Mater. Interfaces 2014, 6, 11915–11923. [PubMed: 24977302]

(48). Park J; Kim D-H; Kim H-N; Wang CJ; Kwak MK; Hur E; Suh K-Y; An SS; Levchenko A Directed Migration of Cancer Cells Guided by the Graded Texture of the Underlying Matrix. Nat. Mater 2016, 15, 792–801. [PubMed: 26974411]

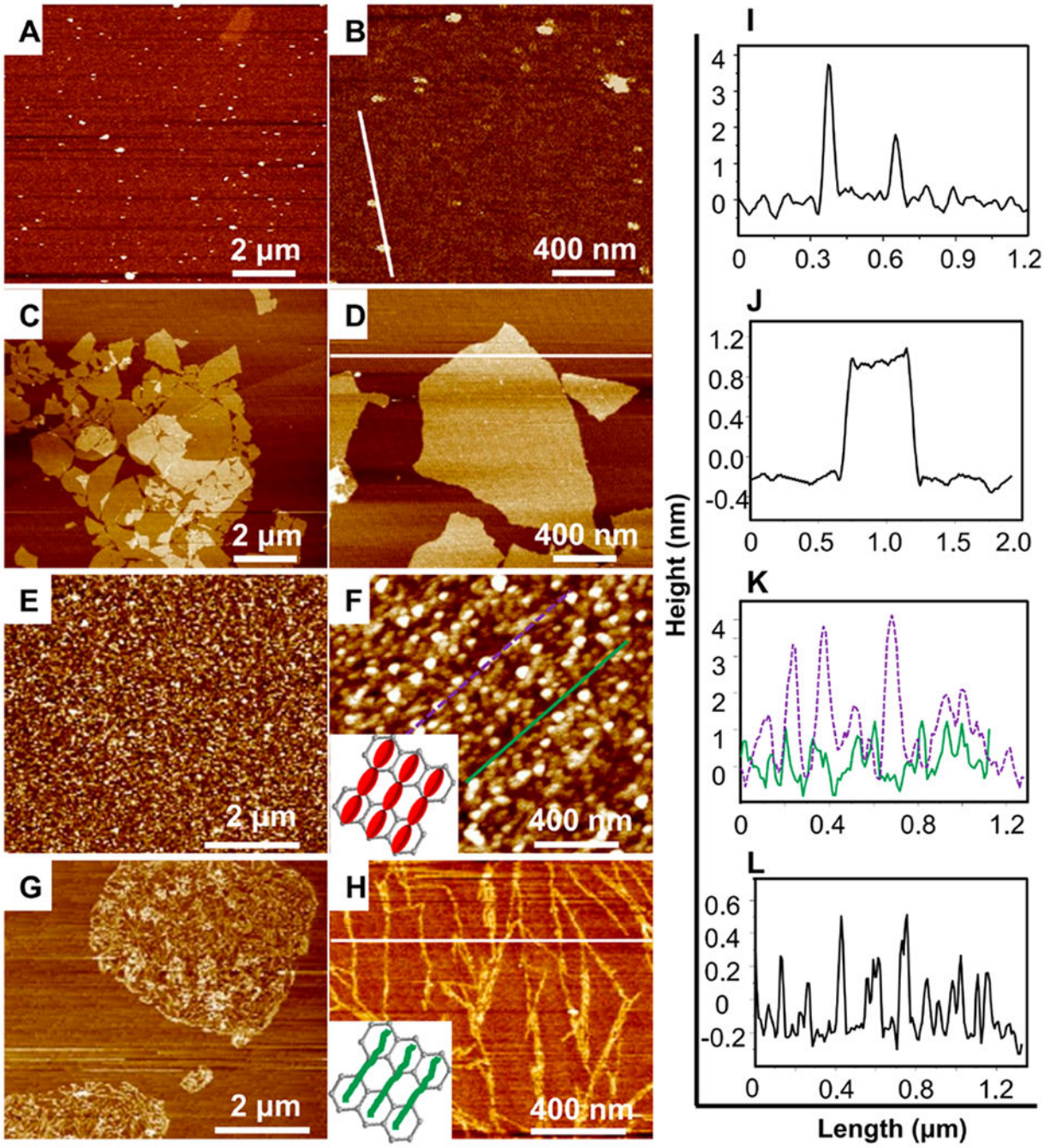


**Figure 1.**

Morphologies of SF nanoparticles and the assembled nanofibers on GO nanosheets. (A–H) AFM morphology of SF nanoparticles (A,B), GO nanosheets (C,D), and SF/GO solutions with GO contents of 2% (E,F) and 10% (G,H). (B,D,F,H) Magnified view of a typical area in (A,C,E,G), respectively. When the GO content was 2%, the schematic of necklace-like SF nanofibrils was shown at the bottom left of (F), and the schematic of solid SF nanofibrils when GO contents was 10% was shown at the bottom left of (H). The section analysis in (I) shows that SF nanoparticles had a height of 3.7 or 1.8 nm. The section analysis in (J) shows

that a GO nanosheet had an extremely thin and smooth characteristic surface with the height about 1 nm. The section analysis in (K) shows that at 2% of GO, the height of necklace-like SF particle assemblies at the thicker area [purple dotted line in (F)] can reach up to 4 nm (as shown by the purple dotted curve) and the height of those at the thinner area [green line in (F)] was about 1.5 nm (as shown by the green curve). The section analysis in (L) shows that when GO content is increased to 10%, the newly formed SF nanofibrils had a height of 0.3 nm.

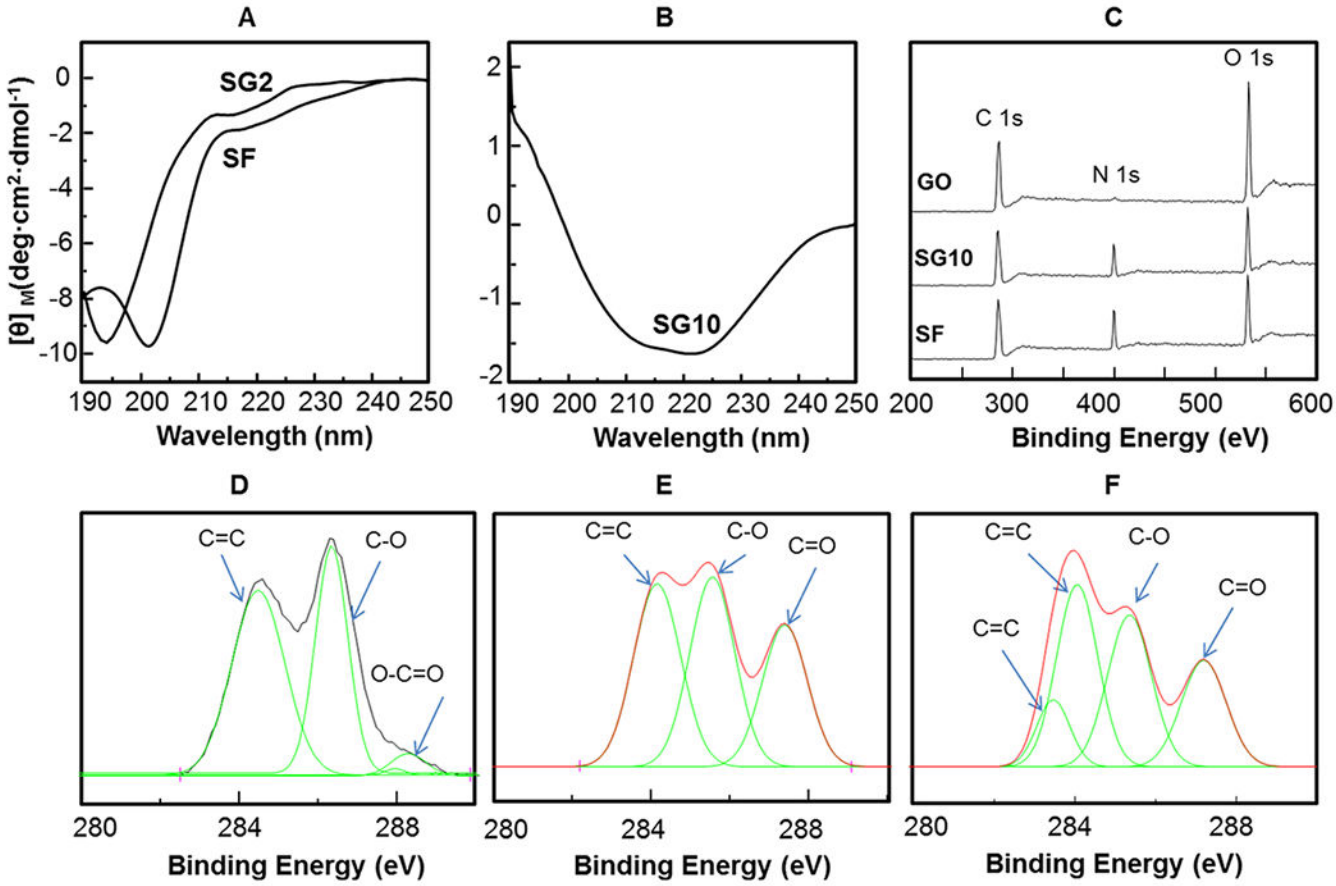


**Figure 2.**

Structural changes of SF molecules and GO templates in the one-pot reaction solutions. (A,B) CD spectra of SG2 and SF (A) and SG10 (B). (C–F) XPS spectra of GO, SG10, and SF. CD spectra proved that the secondary structure of SF can be controlled by changing the GO content. XPS spectra show almost no nitrogen in the GO solution and the SG10 had an emerging N peak because of the contribution of the amino acids from SF. The high-resolution C 1s spectra of GO (D), SG10 (E), and SF (F) show that GO was reduced by SF molecules in SG10 solution.

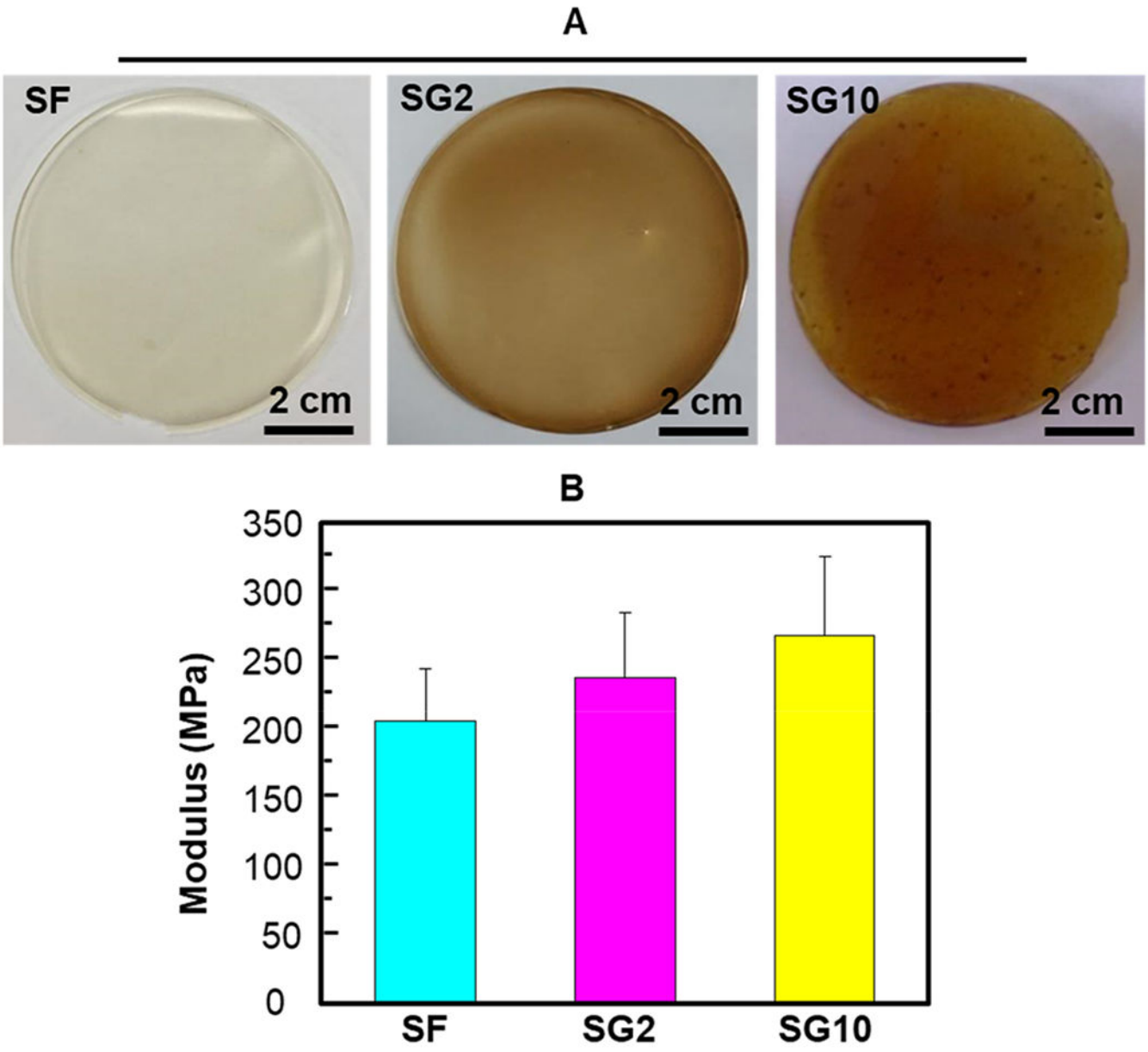


**Figure 3.**

Surface morphology and mechanical characteristics of the SF/GO films. (A–B) Digital photographs (A) and Young's modulus (B) of the SF film, SG2 film, and SG10 film. By regulating the content of GO, the mechanical characteristics of SF film can be changed correspondingly.

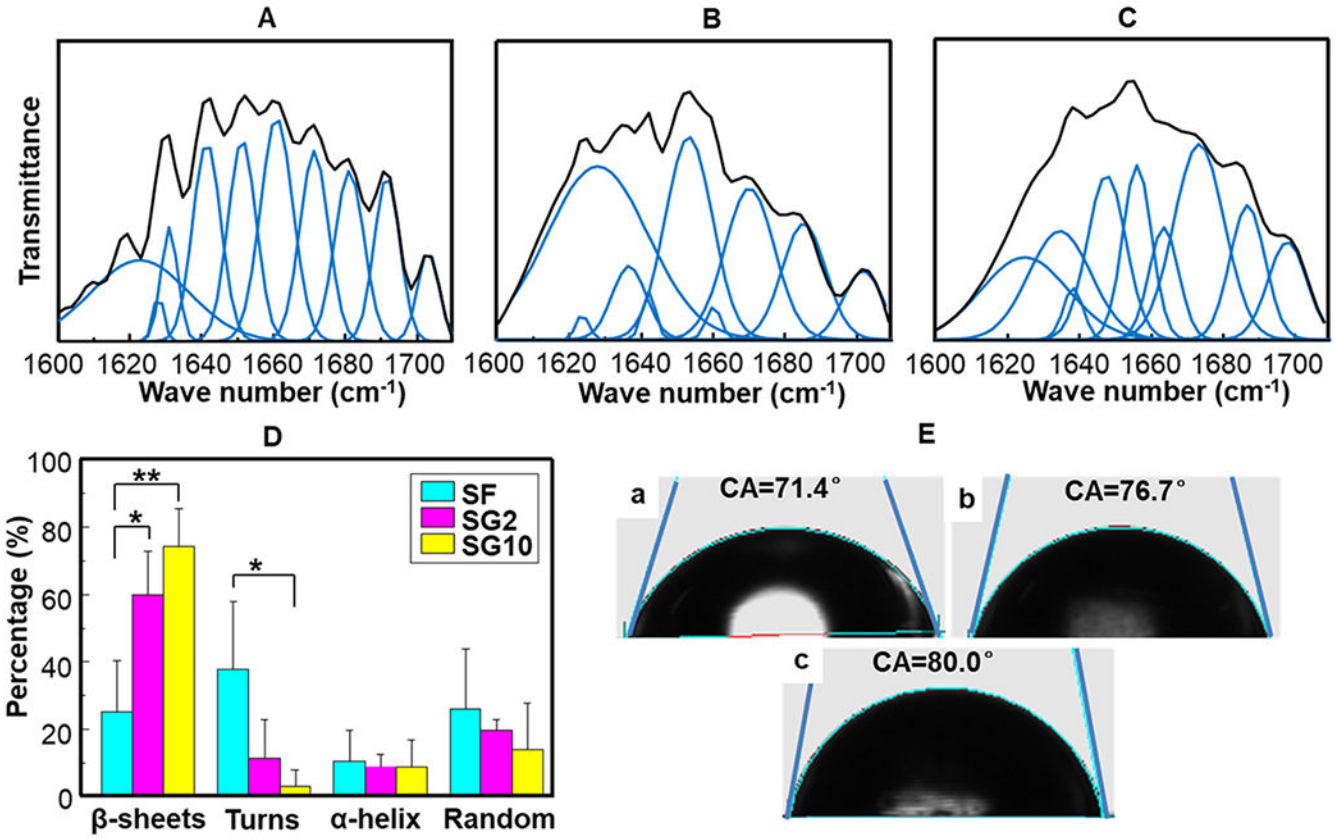


**Figure 4.**

Secondary structure and surface properties of the SF film and composite SF/GO films. (A–C) Curve fitting result of FTIR spectrum in the amide I spectra of SF (A), SG2 (B), and SG10 (C). (D) Percentage of beta-sheets, turns, alpha-helix, and random coils determined by amide I deconvolution of SF/GO films. (E) Contact angle measurements of SF film (a), SG2 film (b), and SG10 film (c). $*P < 0.05$, $**P < 0.01$, data are presented as mean ± SD, $n = 3$.

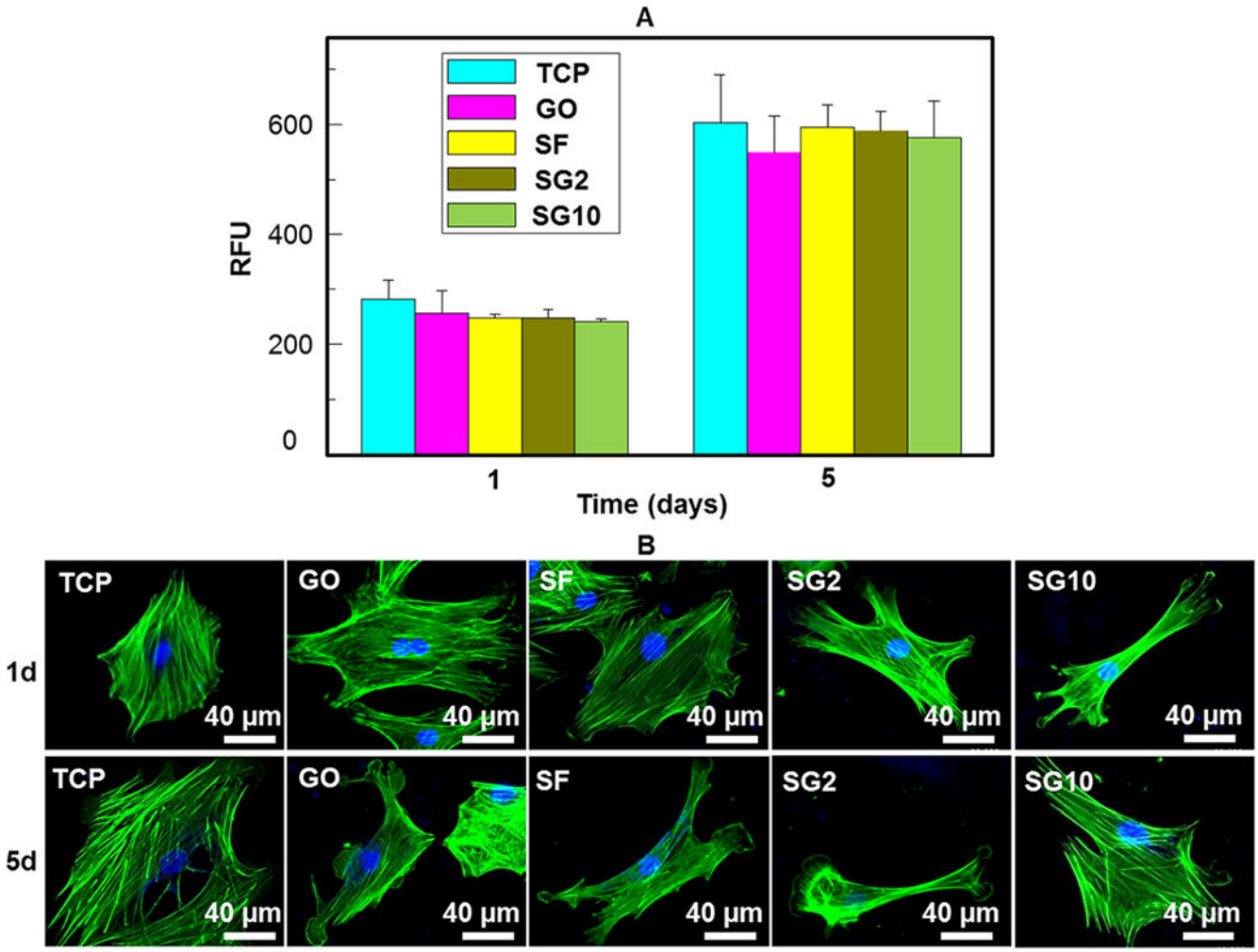


**Figure 5.**

Proliferation and morphology of human MSCs on the SF/GO films. (A) RFU can reflect the number of cells on SF/GO films. The population doubling time was about 5 d. (B) Morphology of human MSCs on TCP, GO coating, SF film, SG2 film, and SG10 film with actin stained in green by Alexa Fluor 488 phalloidin and nuclei stained by DAPI after the cells were cultured for 1 and 5 d.

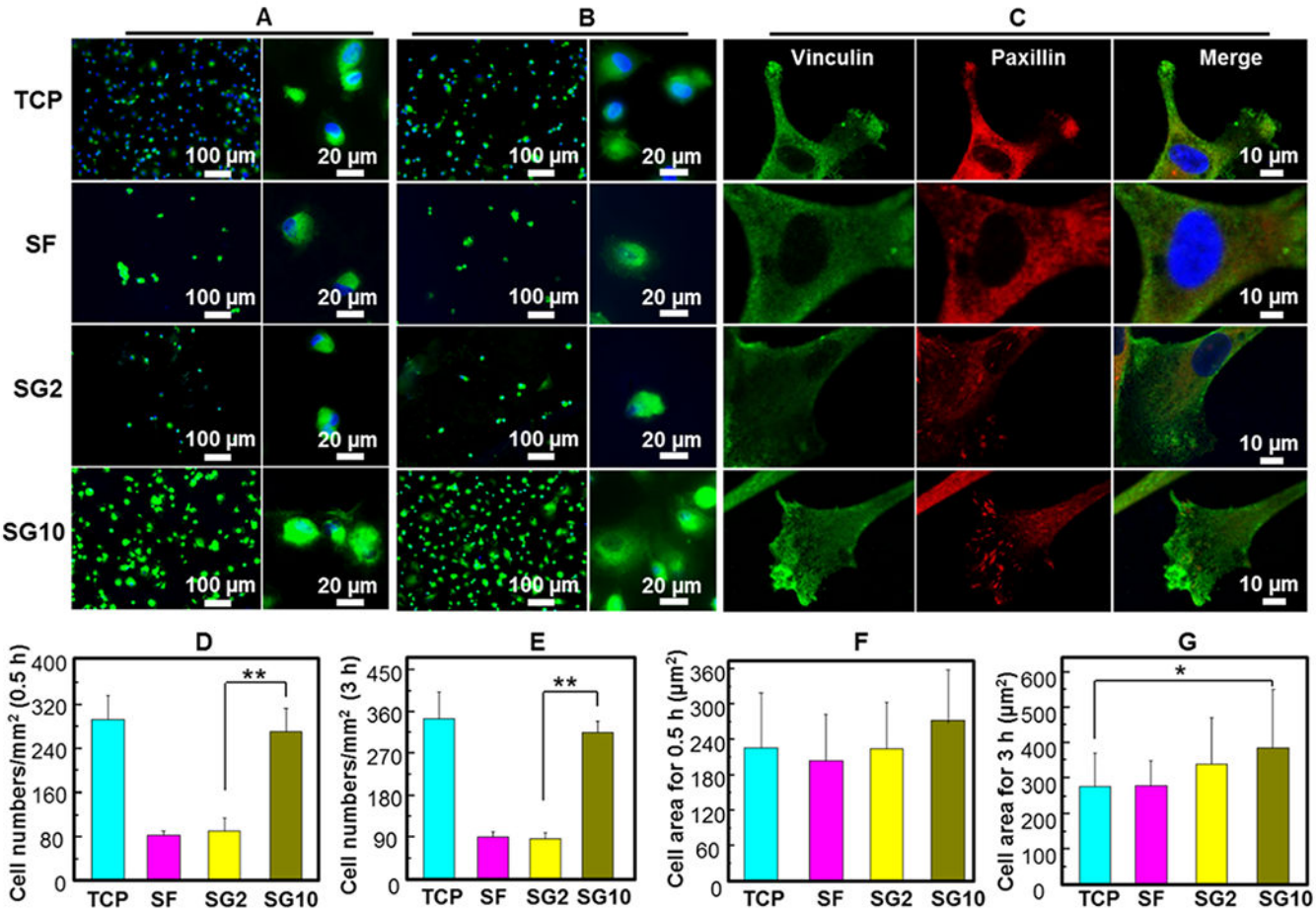


**Figure 6.**

Evaluation of cell adhesion effect and expression of adhesion-associated proteins seeded on the SF/GO films. (A,B) Adhesion morphology of MSCs on TCP, SF film, SG2 film, and SG10 film for 0.5 (A) and 3 h (B). (C) Immunofluorescence staining of two adhesion-associated proteins including vinculin and paxillin. (D,E) Quantitative analysis of cell numbers in (A,B), respectively. (F,G) Quantitative analysis of each cell adhesion area in (A,B), respectively. $^{**}P < 0.01$, data are presented as mean ± SD, $n = 5$.

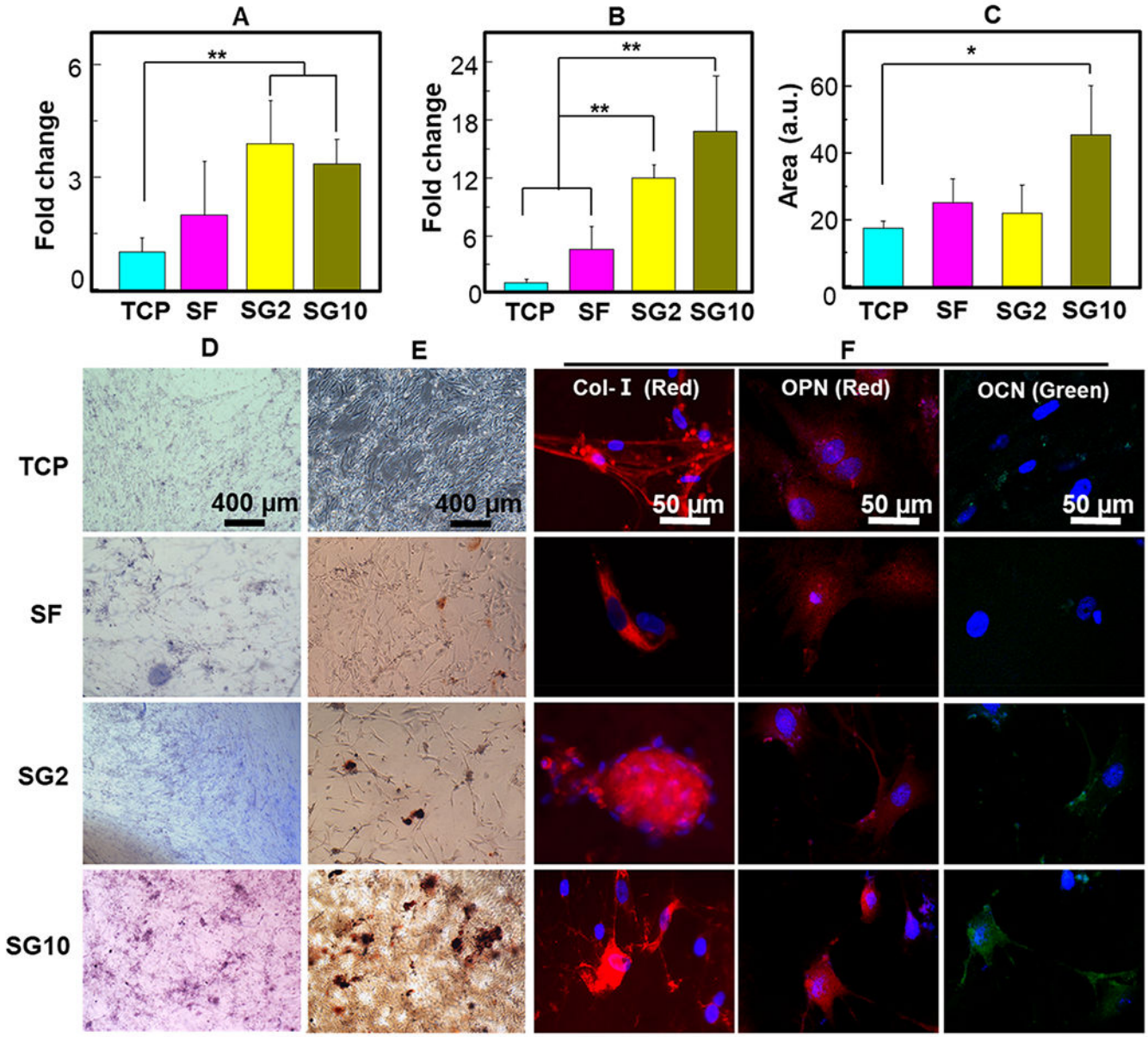


**Figure 7.**

Assessment of osteogenic differentiation efficiency of human MSCs on the SF/GO films cultured in the osteogenic induction medium or the normal medium. (A,B) Levels of mRNA for Itg$\alpha$2 (A) and COLI (B) of human MSCs for 14 d cultured in the osteogenic induction medium. (D,E) ALP staining (D) and alizarin red staining (E) of MSCs cultured on TCP, SF film, SG2 film, and SG10 film for 14 d in the normal medium. (C) Quantitative result of alizarin red staining in (E). Immunofluorescence images (F) of COLI, OCN, and OPN proteins in human MSCs seeded for 14 d cultured in the normal medium. OCN was stained by Alexa Fluor 488-labeled antibody (green). COLI and OPN were stained by Alexa Fluor 594-labeled antibody (red). Cell nuclei were stained with DAPI (blue). *$P < 0.05$, **$P < 0.01$, data are presented as mean ± SD, $n = 4$.

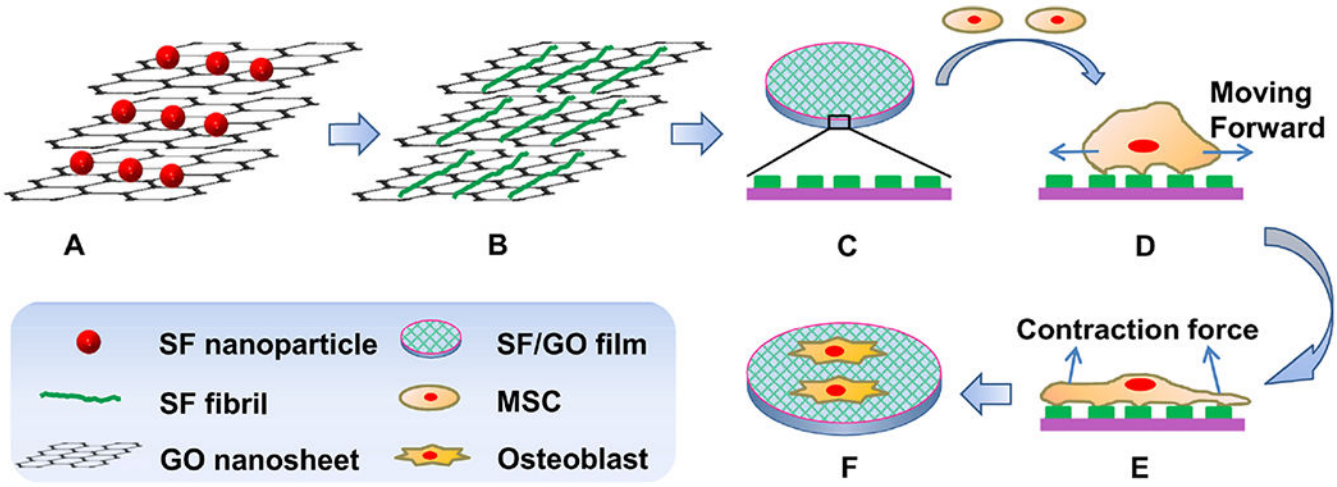


**Scheme 1.**

Schematic Diagram Depicting the Formation of SF Nanofibrils by the GO Template and the Use of the Resultant Nanofibrous Matrix as a Platform for Osteogenic Differentiation of MSCs; (A) Spherical SF Nanoparticles and GO Nanosheets Were Mixed with GO Content between 2 and 10% by a One-Pot Reaction; (B–C) after the Reaction, Spherical SF Nanoparticles Were Assembled into Nanofibrils on the GO to Cover the Surface of GO Nanosheets (B), Forming an SF/GO Film (C); (D) Human MSCs Were Cultured on and Attached to the SF/GO Film; (E) Cells Were Dynamically Stretched on the SF/GO Film through the Reassembly of Cytoskeleton Proteins; (F) in the Absence of Osteogenic Inducers, MSCs Cultured on the SF/GO Film Showed Enhanced Early Adhesion and Specific Differentiation toward Osteoblasts

**Table 1.**

Primer Sequences Used for Reverse Transcription-Polymerase Chain Reaction Gene Expression Analysis

| genes | 5′–3′ | primers |
|---|---|---|
| GAPDH | forward | TGACGCTGGGGCTGGCATTG |
| | reverse | GGCTGGTGGTCCAGGGGTCT |
| collagen I | forward | ATGGATTCCAGTTCGAGTAGGC |
| | reverse | CATCGACAGTGACGCTGTAGG |
| integrin $\alpha 2$ | forward | CCGACAGGGGTTATCATAGGCA |
| | reverse | CATTCACCACACCAGCGAGC |